Geometry and water accessibility of the inhibitor binding site of Na$^+$-pump: Pulse- and CW-EPR study

Erika Aloi,[1] Jin-Hua Guo,[2] Rita Guzzi,[1] Ren-Wang Jiang,[2,*] Lucy Kate Ladefoged,[3] Derek Marsh,[4] Mikael Esmann,[3] Rosa Bartucci,[5,*] and Natalya U. Fedosova[3,*]

[1]Department of Physics, Molecular Biophysics Laboratory, University of Calabria, Rende, Italy; [2]Guangdong Province Key Laboratory of Pharmacodynamic Constituents of TCM and New Drugs Research, College of Pharmacy, Jinan University, Guangzhou City, P. R. China; [3]Department of Biomedicine, Aarhus University, Aarhus, Denmark; [4]Max-Planck-Institut für biophysikalische Chemie, Göttingen, Germany; and [5]Department of Chemistry and Chemical Technologies, Molecular Biophysics Laboratory, University of Calabria, Rende, Italy

ABSTRACT Spin labels based on cinobufagin, a specific inhibitor of the Na,K-ATPase, have proved valuable tools to characterize the binding site of cardiotonic steroids (CTSs), which also constitutes the extracellular cation pathway. Because existing literature suggests variations in the physiological responses caused by binding of different CTSs, we extended the original set of spin-labeled inhibitors to the more potent bufalin derivatives. Positioning of the spin labels within the Na,K-ATPase site was defined and visualized by molecular docking. Although the original cinobufagin labels exhibited lower affinity, continuous-wave electron paramagnetic resonance spectra of spin-labeled bufalins and cinobufagins revealed a high degree of pairwise similarity, implying that these two types of CTS bind in the same way. Further analysis of the spectral lineshapes of bound spin labels was performed with emphasis on their structure (PROXYL vs. TEMPO), as well as length and rigidity of the linkers. For comparable structures, the dynamic flexibility increased in parallel with linker length, with the longest linker placing the spin label at the entrance to the binding site. Temperature-related changes in spectral lineshapes indicate that six-membered nitroxide rings undergo boat-chair transitions, showing that the binding-site cross section can accommodate the accompanying changes in methyl-group orientation. D$_2$O-electron spin echo envelope modulation in pulse-electron paramagnetic resonance measurements revealed high water accessibilities and similar polarity profiles for all bound spin labels, implying that the vestibule leading to steroid-binding site and cation-binding sites is relatively wide and water-filled.

SIGNIFICANCE The extracellular access channel for the cations of the Na$^+$,K$^+$-ATPase overlaps with the enzymes' binding site for cardiotonic steroids. Attachment of a spin label to bufadienolide (a cardiotonic steroid) core through linkers of different lengths places the reporting group in various positions in this cavity and allows characterization of its size and properties by electron paramagnetic resonance techniques. The ability of the nitroxide rings of the probes to undergo chair-boat conformational transitions as well exposure of all spin labels (independently of the linker lengths) to high water concentration revealed that the cavity is wide and water-filled. Docking simulations allow us to relate these findings to a crystal structure of the E2P conformation of the Na$^+$,K$^+$-ATPase.

INTRODUCTION

The Na$^+$,K$^+$-ATPase, or sodium pump, is a complex of three integral membrane proteins. The α-subunit contains the hydrolytic site and all ligand-binding sites, spans the membrane 10 times, and has a large intracellular part, whereas accessory (β) and regulatory (γ) subunits each

possess one transmembrane helix (1,2). The enzyme plays a central role in the homeostasis of animal cells (3); it maintains ion gradients across the plasma membrane and may participate in signal transduction by initiating different cascades within the cell. Na$^+$,K$^+$-ATPase is the primary pharmacological receptor for cardiotonic steroids (CTSs, cardiac glycosides). The ability of these compounds to inhibit Na$^+$,K$^+$-ATPase, with concomitant effect on intracellular Ca^{2+}-concentration, has long been the rationale behind use of CTSs in treatment of heart failure. The newly described receptor function of the enzyme, however, opens up the possibility for other mechanisms of inhibitor action and makes the Na$^+$,K$^+$-ATPase an attractive target for

drug development. The CTSs, natural inhibitors of the enzyme, are used as "lead substances" for modifications that increase specificity in their action.

Bufalin and cinobufagin, two major components in traditional Chinese medicine, both belong to bufadieno-lides, a subgroup of CTSs with significant pharmacological activity against certain types of cancer. There are, however, reports that the cytotoxic effects are not proportional to the known inhibitory effects on Na^+,K^+-ATPase activity. For example, bufalin effectiveness as an anti-cancer drug was lowest in a row of its derivatives if estimated from the ratio of $IC_{50}^{Na,K\ pump}/IC_{50}^{proliferation}$ (4).

The absence of the direct correlation between inhibition of the pump activity and the effect on cell proliferation suggests either the existence of CTS targets other than the Na,K-ATPase or different binding modes of CTSs and the Na,K-ATPase. This report addresses the second possibility and compares modes of interaction of spin-labeled bufalin and cinobufagin derivatives with the Na^+,K^+-ATPase.

Our custom synthesized CTS derivatives allowed us to address another issue concerning the environment of the sugar units attached to the steroid core of many CTSs. Thus, a well-established method for time-resolved measurements of CTS interactions with the enzyme is based on the ability of anthro-ylouabain to change its fluorescence upon binding (5). This spectral change suggests that the fluorophore attached to rhamnose experiences a hydrophobic environment of the site. At the same time, the crystallographic data on the CTS complexes with the Na^+,K^+-ATPase (6–8) reveal that sugar units of the glycosylated representatives reside in a wide cavity exposed to solvent. The most distant of them might reach as far as the β-subunit of the enzyme. The fact that this part of the structure is not well resolved keeps the possibility for temporary interactions with the amino acid residues open. To obtain the detailed description of interaction between the Na^+,K^+-ATPase and individual CTSs, it is therefore desirable to complement crystallographic information with independent evaluation of the polarity of the site and of the mobility of the distal sugar units.

Earlier, we established the potential of continuous-wave electron paramagnetic resonance (CW-EPR) spectroscopy for characterizing the binding site of Na^+,K^+-ATPase under physiological conditions (9). For this work, we have designed and synthesized pairwise, congruent spin labels with bufalin and cinobufagin steroid cores having different lengths of the spacer arm between the EPR-active nitroxide group (-NO) and the steroid core, and we have introduced five- (i.e., PROXYL) as well as six-membered (i.e., TEMPO) nitroxide rings (Fig. 1). Their use allows access to different regions within the binding site, whereas application of high concentrations of the competitor ouabain clearly discriminates between specific and nonspecific interactions (9). The results reveal no steroid core-related differences in binding modes of the two spin-label series. Data from both electron spin echo envelope modulation by D_2O (D_2O-ESEEM) and

CW-EPR provide information on 1) water accessibility, 2) environmental polarity, and 3) rotational mobility in the temperature range between 5 and 50°C for these probes in both specifically and nonspecifically bound states. Combined with molecular docking of these probes, based on the crystal structure of the bufalin-Na^+,K^+-ATPase complex, EPR results indicate that the cavity at the entrance of the CTS binding site is of high polarity, is exposed to water, and allows various degrees of mobility of the ligands. The cavity is the very distal part of the pathway connecting cation-binding sites with the extracellular environment. Its most proximal part, or access channel, was earlier described as wide and water-filled based on pump current measurements and molecular dynamics simulations of the truncated enzyme (without ectodomain of the β-subunit) (10). Our results present the experimental proof that this inference is now valid for native enzyme.

MATERIALS AND METHODS

General synthetic procedures

Bufadienolides (starting materials), viz. cinobufagin and bufalin, were purchased from Shanxi Chenguang Biological Technology (Shanxi, China) with purity ≥98% (high-performance liquid chromatography (HPLC)). Pyrrolidine-type and piperidine-type nitroxides, specifically 3-carboxy-2,2,5,5-tetramethylpyrrolidine-1-oxyl and 4-hydroxy-2,2,6,6-tetramethyl-piperidine, respectively, were purchased from Shanghai Aladdin Reagent (Shanghai, China) and used without further purification. All commercially available reagents were used as received unless stated otherwise (J&K Scientific, Beijing, China). Synthetic procedures for all novel, to our knowledge, compounds and their detailed characterization are described in the Supporting materials and methods, Figs. S1–S17, Schemes S1 and S2, and Tables S1 and S2.

Na^+,K^+-ATPase and its interaction with the spin labels

Na^+,K^+-ATPase from pig kidney microsomal membranes was purified by treatment with sodium dodecyl sulfate, followed by differential centrifugation (11). The inhibitory effects of bufalin and cinobufagin spin labels on Na^+,K^+-ATPase were determined essentially as reported previously (9). Results are expressed in percent of the Na^+,K^+-ATPase activity in the absence of inhibitor. Kinetic analysis was performed as described in (6).

Sample preparation for CW-EPR

Samples for CW-EPR experiments were prepared as described in (9). This protocol ensures that samples in the absence of ouabain contain a negligible amount of nonspecifically bound spin labels. Calculation of the amount of nonspecifically bound spin label and its relative contribution to the spectrum is shown in Figs. 4, B and C, and 6 B of (9).

Sample preparation for D_2O-ESEEM pulse EPR

Membrane fractions of the Na^+,K^+-ATPase were first transferred to a 250 mM sucrose, 20 mM histidine, 0.9 mM EDTA (pH 7.0) buffer containing D_2O by triple washing and centrifugation procedure. Binding of spin labels to enzyme was carried out essentially as for the CW-EPR
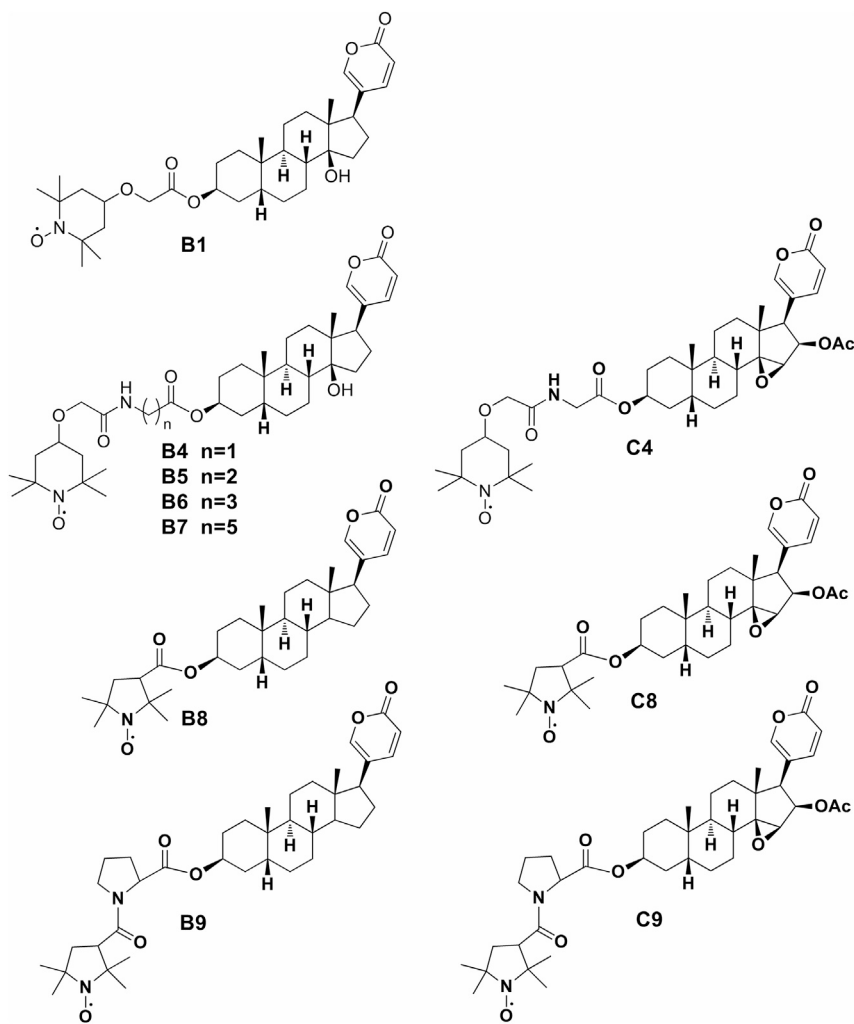
FIGURE 1 Structures of spin-labeled cinobufagins (**C**) and bufalins (**B**).

experiments, except that D$_2$O instead of H$_2$O was used throughout for buffers, ouabain solutions, etc.

Samples were frozen and not thawed before EPR spectroscopy. The same samples were used for CW-EPR experiments at −196°C.

EPR spectroscopy

Conventional CW-EPR spectra were acquired on a 9-GHz ESP-300 spectrometer equipped with ER-4201 rectangular TE$_{102}$ cavity and ER-4111VT temperature controller (all from Bruker Corporation,Billerica, MA). For measurements at −196°C, 4-mm sample tubes were first frozen rapidly in liquid nitrogen and then introduced into a finger Dewar containing liquid nitrogen. For measurements at higher temperatures, sample capillaries were inserted in a standard 4-mm EPR quartz tube containing light silicone oil to avoid thermal gradients, and spectra were registered on heating. Spectra were recorded at a microwave power well below saturation with 100-kHz field modulation and typically were accumulated 16–25 times to improve the signal/noise ratio.

Pulsed-EPR data were collected at −196°C on a Bruker ELEXSYS E580 Fourier transform-EPR spectrometer at 9 GHz using a MD5 dielectric resonator (Bruker) and CF 935P cryostat (Oxford Instruments, Abingdon, UK). To obtain ESEEM spectra, three-pulse, stimulated echo ($\pi/2$-τ-$\pi/2$-T-$\pi/2$-τ-echo) decays were recorded by using microwave pulse widths of 12 ns, with the microwave power adjusted to give $\pi/2$-pulses. The time delay, T, be-

tween the second and third pulses was incremented from 20 ns in 700 steps of 12 ns, and the interpulse separation, τ, between the first and second pulses was fixed at 168 ns to maximize the deuterium and proton modulations simultaneously. The magnetic field was set to the maximum of the EPR absorption. A four-step phase-cycling program was used to eliminate unwanted echoes. For obtaining standardized ESEEM intensities, the time-dependent echo amplitudes were processed according to a protocol developed previously (12,13).

For three-pulse ESEEM experiments, samples were frozen rapidly in liquid nitrogen and then quickly transferred to the precooled cavity at −196°C.

Docking procedures

Protein preparation

The protein model was prepared from Protein Data Bank, PDB: 4RES ($\alpha1\beta1\gamma$ subunits) (8) using the Protein Preparation Wizard (14) in Maestro (Schrödinger Suite 2019) as described elsewhere (15). The resulting model included disulfide bridges between CysB126-CysB149, CysB159-CysB175, and CysB213-CysB276; neutral AspA808, AspA926, GluA244, GluA327, GluA779, and GluA954; histidines HisB212, HisA286, HisA517, HisA550, HisA613, HisA659, HisA678, HisA875, and HisA912 modeled as the ε-tautomer; and AspA369 as phosphorylated, whereas all other residues were modeled in the default state.

Spin-labeled bufadienolide preparation

Spin-labeled bufalin compounds **B1**, **B4**, **B7**, **B8**, and **B9**, as well as spin-labeled cinobufagin compound **C8**, were all based on bufalin from PDB: 4RES (8) and manually extended using the build panel in Maestro (Schrödinger Suite 2019). The protonation state of each compound was assessed using Epik (16) and, because radicals are not supported by the force field, all compounds were modeled with the nitroxide oxygen as negatively charged.

The compounds were then minimized using a conjugant-gradient algorithm in 5000 steps and subjected to a conformational search using a mixed torsional and low mode sampling algorithm as implemented in MacroModel (Schrödinger Suite 2019). Both calculations were performed using the optimized potentials for liquid simulations (OPLS)-2005 force field (17). The lowest-energy conformation of each compound was used in subsequent docking calculations.

XP docking calculation

The compounds were docked flexibly into the Na$^+$,K$^+$-ATPase by using the XP docking procedure in Glide (18) (Schrödinger Suite 2019). The centroid of the binding site was defined based on the cocrystallized bufalin molecule. The inner box was $1.0 \times 1.0 \times 2.0$ nm (x, y, z), and the outer box was $4.6 \times 4.6 \times 5.6$ nm. These box sizes were necessary for obtaining poses of the large ligands within the binding site. Additionally, to increase sampling, the following settings were altered from the default: the Epik state penalties were removed from the score, an energy window of 126 kJ mol^{-1} (30 kcal/mol) for ring sampling was allowed, an energy window of 837 kJ mol^{-1} (200 kcal/mol) was allowed for pose retention in the first phase of the docking calculation, and the expanded sampling option was used. For each ligand, a maximum of 50 poses were allowed in the final output. Calculations were performed using the OPLS-2005 force field (17).

Water-accessible volume calculations

The water-accessible volume within the CTS binding site was calculated using trj_cavity (19). In the calculation, the binding site was lined by protein in five out of six dimensions (positive and negative direction of z, y, and z dimensions). The coordinates of K$^+$ in site II were taken as a seed point for starting the site calculation with a cutoff distance of 8 Å to limit the calculation.

RESULTS

Properties of the bufalin and cinobufagin spin labels

3β-OH of cinobufagin and bufalin steroid cores was chosen for derivatization and attachment of a nitroxide group in the design of these EPR probes. This ensures binding within the specific site, whereas spacer arms varying in length and structure determine the position of the spin label in the binding cavity. Fig. 1 shows structures of seven synthesized EPR probes, and Figs. S1–S17 and Tables S1 and S2 summarize the chemical parameters of the EPR probes.

Inhibitory effects of bufalin and cinobufagin spin labels on Na$^+$,K$^+$-ATPase

As shown by Guo et al. (9), derivatizing the 3β-OH of cinobufagin did not prevent specific binding of the product compounds in the CTS binding site. This was also the case for synthesis of spin labels based on bufalin. Residual Na$^+$,K$^+$-ATPase hydrolytic activities after incubation with varying concentrations of each derivative are shown in Fig. S18, and the kinetic parameters for inhibition are summarized in Table S3. All compounds exhibit the kinetic behavior observed for bufalin and cardenolide aglycons in this particular experimental setup (8). The values of K_{Diss} are relatively low: all compounds are high-affinity inhibitors of the Na$^+$,K$^+$-ATPase. However, the Na$^+$,K$^+$-ATPase-inhibitor complex dissociates with two different rates: a fast and a slow one relative to duration of the activity measurement. According to Table S3, the fast-dissociating, (i.e., low-affinity) complex represents maximally 1/3 of the total amount of inhibited enzyme (e.g., spin label **B5**). Our understanding of this phenomenon based on molecular dynamics is described elsewhere (15). It is unimportant for interpreting the EPR experiments because samples are prepared under equilibrium conditions of ligand binding without dilution. Both fast- and slow-dissociating complexes have bound ligand and inhibited Na$^+$,K$^+$-ATPase. Because of the significant excess of protein (12 μM) over ligand (4 μM), the amount of nonspecifically bound ligand in EPR experiments is negligible in all cases (see (9) for further details).

CW-EPR spectroscopy

CW-EPR spectra of Na$^+$,K$^+$-ATPase membranes at 26°C, with and without ouabain, are shown for spin-labeled bufalins **B9**, **B8**, and **B4** in the upper row of Fig. 2.

Single-component spectra with differing degrees of anisotropy are seen for the three spin-labeled bufalins (**B**) in Na$^+$,K$^+$-ATPase membranes. This indicates different extents of averaging the spectral anisotropy by rotational diffusion, for the six spin labels. (By spectral anisotropy, we mean that spectral positions depend on angular orientation of the magnetic field to the nitroxide axes shown in Fig. S22. For a nonaligned sample, this causes a spread in spectral positions that corresponds to different orientations of the nitroxide axes to the spectrometer field—a so-called powder distribution. See, e.g., (20).) The **B9** structure includes a rigid five-membered heterocycle linking the PROXYL ring with the lactone-steroid core. In the absence of ouabain (*solid lines*), this five-membered-ring (i.e., PROXYL) nitroxide displays a wide anisotropic spectrum with sharp outer lines at low- and high-field and peak separation, $2A_{max}$, of 6.85 mT. The five-membered-ring bufalin **B8** has the shortest spacer arm between nitroxide spin-label moiety and lactone-steroid core. Its spectrum displays a lower degree of anisotropy compared with that of **B9**, with $2A_{max}$ of 6.34 mT and broader outer extrema. An anisotropic spectrum with yet lower $2A_{max}$-value of 6.09 mT is displayed by the six-membered-ring bufalin **B4** in Na$^+$,K$^+$-ATPase membranes.

Control spectra in the presence of excess ouabain (Fig. 2, *upper row*, *dashed line*) indicate that all spin-labeled
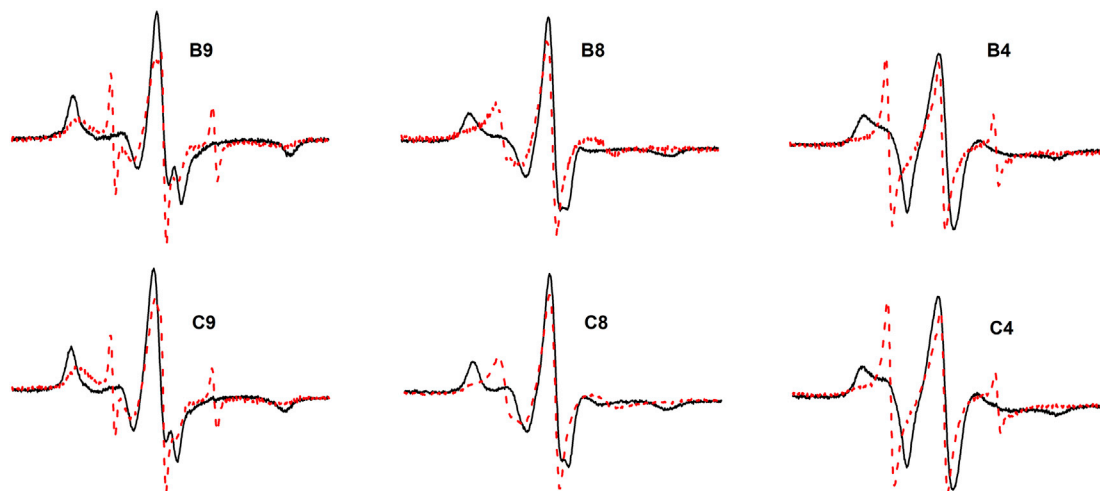
FIGURE 2   Upper row: CW-EPR spectra at 26°C of bufalin steroids **B9**, **B8**, and **B4** in Na$^+$,K$^+$-ATPase membranes in the absence (*full line*) and presence (*dashed line*) of 0.5 mM ouabain. Lower row: corresponding CW-EPR spectra of cinobufagin steroids **C9**, **C8**, and **C4**. Central field = 332.5 mT, sweep width = 10 mT. To see this figure in color, go online.

bufalins additionally sample nonspecific loci in Na$^+$,K$^+$-ATPase membranes. We discussed this previously in (9); see also (21). The spectra are a superposition of components characteristic of different rotational mobilities. For **B9**, an anisotropic component from the lipid environment directly adjacent to the Na$^+$,K$^+$-ATPase protein is clearly evident,

in addition to a sharp isotropic triplet from spin label partitioned into the aqueous phase. The multicomponent spectrum of **B8** shows again an outer anisotropic component from the protein-lipid interface, which here overlaps in the central region with a less anisotropic component from the fluid-bilayer environment of the membrane (22,23). Finally, the spectrum of **B4** consists of a large amount of an isotropic sharp three-line component (from the aqueous bulk phase) superimposed on residual contributions of anisotropic components characteristic for the lipid and lipid-protein environments of the membrane.

Interestingly, almost identical spectral features characterize the CW-EPR spectra of the corresponding cinobufagin steroids **C9**, **C8**, and **C4** in Na$^+$,K$^+$-ATPase membranes, in both the absence and presence of ouabain (see *spectra* in the *lower panel* of Fig. 2). Note that the spectral components identified above for both specific and nonspecific sites of spin-labeled bufalins agree with those characterized previously for other spin-labeled variants of cinobufagin (9).

CW-EPR spectra of six-membered-ring bufalin spin labels with progressively longer linking arm, namely **B1**, **B4**, **B5**, **B6**, and **B7**, are shown in Fig. 3. Control spectra in the presence of ouabain are also given (*dashed lines*). The spectra in Fig. 3 display the three ^{14}N-nitroxide hyperfine lines with different degrees of anisotropy. The spectral anisotropy decreases with length of the linker from **B4** onward by progressively introducing intervening methylene groups. Indeed (except for **B1**), the total spectral width and the linewidths at low and high fields decrease from **B4** to **B5**, **B6**, and **B7**. At the same time, the control spectra in presence of ouabain approach isotropic patterns with gradually decreasing residual anisotropy. This is superimposed on a more anisotropic component that is most evident as a wing at low field
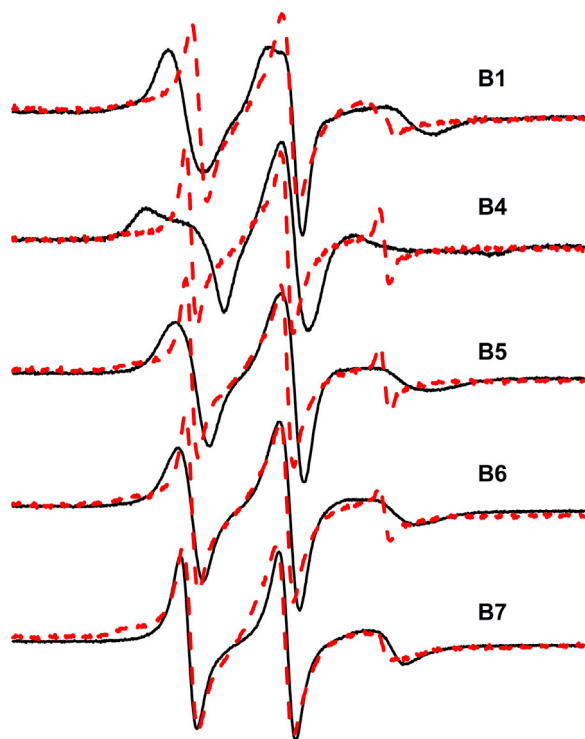

FIGURE 3   CW-EPR spectra at 26°C of spin-labeled bufalins **B1**, **B4**, **B5**, **B6**, and **B7** in Na$^+$,K$^+$-ATPase membranes in the absence (*full line*) and presence (*dashed line*) of ouabain. Central field = 332.5 mT, sweep width = 10 mT. To see this figure in color, go online.
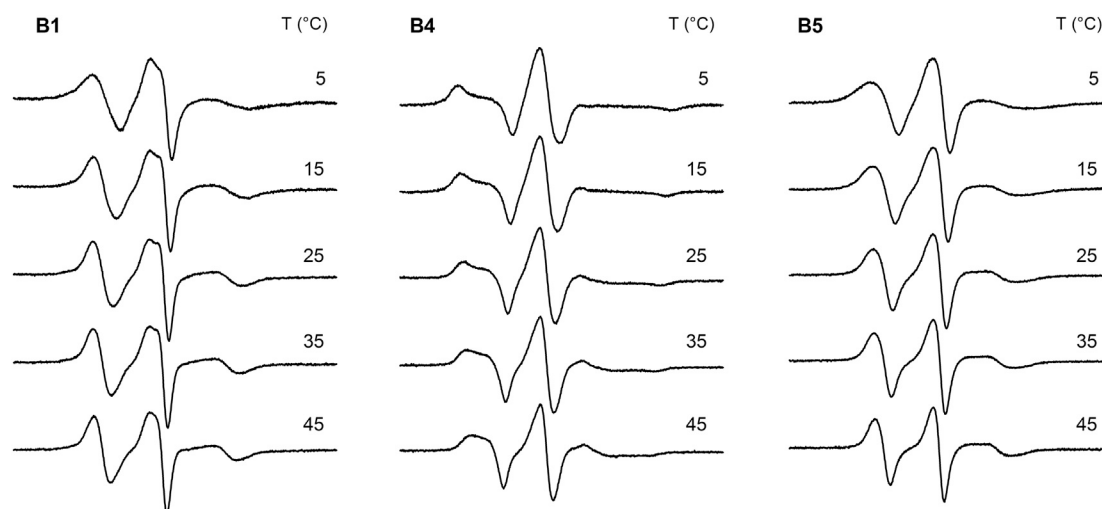
FIGURE 4 Temperature dependence of the CW-EPR spectra from spin-labeled bufalins **B1**, **B4**, and **B5** in Na^+,K^+-ATPase membranes. Central field = 332.5 mT, sweep width = 10 mT.

and is accompanied by a small sharp isotropic component from free spin label.

The temperature dependences of the CW-EPR spectra from the three bufalin lactone-steroids **B1**, **B4**, and **B5** in Na^+,K^+-ATPase membranes are shown in Fig. 4. Each nitroxide has the six-membered-ring. For spin-labeled bufalin **B1** with the shorter linker, the spectral anisotropy decreases progressively on increasing the temperature. The apparent outermost peak separation, $2A_{max}$, decreases from 4.90 to 4.68–4.47 mT on going from 5 to 25– 45°C. The CW-EPR spectra of bufalin **B4** are characterized by a larger anisotropy at any temperature. This is consistent with a more immobilized steroid core in the binding site. In this sample, $2A_{max}$ is 6.66 mT at 5°C and reduces to 6.08 at 25°C and to 5.52 at 45°C.
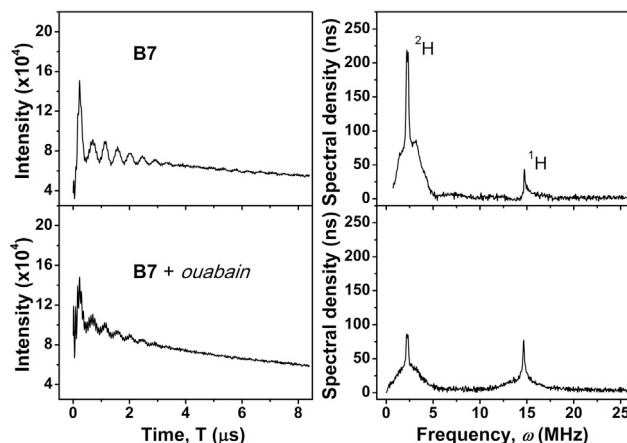

FIGURE 5 Left-hand side: decay curves of the three-pulse electron spin echo amplitude with interpulse spacing, T, for spin-labeled bufalin **B7** in Na^+,K^+-ATPase membranes hydrated in D_2O. Right-hand side: Fourier transform-ESEEM spectra for samples as in the left panel. $T = -196°C$.

CW-EPR spectra from **B5** in the binding site of the Na^+,K^+-ATPase have lineshapes more similar to those of **B1**. We see from their temperature dependence that the spectral anisotropy is slightly lower for the **B5** sample than for **B1** and the effective $2A_{max}$ decreases from 5.02 mT to 4.56–4.34 mT on heating from 5 to 25–45°C.

D_2O-ESEEM of spin-labeled bufalins

Three-pulse ($\pi/2$-τ-$\pi/2$-T-$\pi/2$-τ-echo) D_2O-ESEEM measurements (24,25) were carried out to detect water accessibility in the entrance cavity of the Na^+,K^+-ATPase when sampled by the different nitroxide cardiotonic steroids. As an example, in the left panel of Fig. 5, we show decays of the maximal amplitude of the stimulated echo versus the interpulse spacing, T, at fixed $\tau = 168$ ns, and in the right panel we give absolute-value frequency spectra obtained by Fourier transform for bufalin B7 in the absence and in the presence of ouabain at $-196°C$. Note that numerical Fourier transformation was performed by including specifically the dwell time between data points ($\Delta T = 12$ ns), thus providing machine-independent spectral densities with the dimensions of time (13). The full set of D_2O-ESEEM data is reported in Fig. S19, A and B.

All decays show two modulations: superimposed on a slow oscillation with period of ~ 0.4 μs, there is a rapid oscillation with period of ~ 0.07 μs. The slow modulation is due to dipolar interaction of the label electron spin with the ^2H-nuclear spin of the D_2O molecules, whereas the rapid modulation arises from interactions of the electron spin with nearby ^1H-protons (12).

The absolute-value ESEEM frequency spectra contain lines that are centered around the deuterium ^2H-Larmor frequency at ~ 2.5 MHz and around the proton ^1H-Larmor frequency at ~ 15 MHz. The latter originates from matrix
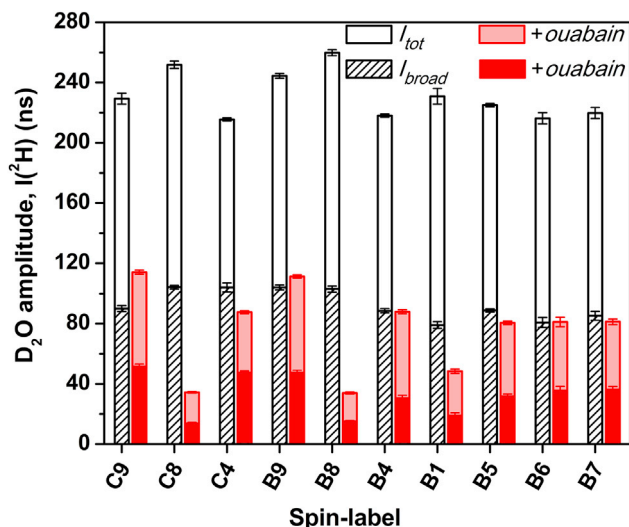
FIGURE 6 Intensity of the total D$_2$O-peak, I_{tot}, and its broad component, I_{broad}, in ESEEM spectra of different spin-labeled cinobufagins (**C**; see Fig. 1 for numbering) and bufalins (**B**) in Na$^+$,K$^+$-ATPase membranes in the absence (*left column*) and presence (*right column*) of ouabain. $T = -196°C$. The data represent averages of three measurements with standard deviations. To see this figure in color, go online.

protons, whereas the former is due specifically to the solvent molecules (12).

In the absence of ouabain, all the samples are characterized by an intense deuterium peak with amplitude in the range 220–260 ns and by a proton peak with amplitude of ~50–60 ns. In the presence of ouabain, the time-domain ESEEM data show a remarkable reduction in amplitude of the D$_2$O modulations and an increase of those from hydrogen nuclei. Correspondingly, the frequency-domain Fourier transform-ESEEM spectra display a reduced intensity of the deuterium peak at 2.5 MHz and a well-defined proton peak of amplitude 80–90 ns at 15 MHz.

TABLE 1 Product of equilibrium constant for H-bonding, *K*, with effective free water concentration, [W], from ^{2}H-ESEEM spectra of cinobufagin and bufalin spin labels from Na$^+$,K$^+$-ATPase membrane dispersions in D$_2$O, and fractions of spin labels that are hydrogen bonded by one and two water molecules

Sample	K[W]	f_{1W}	f_{2W}	+ouabain K[W]	f_{1W}	f_{2W}
C9	0.652	0.478	0.156	0.293	0.350	0.051
C8	0.841	0.496	0.209	0.064	0.113	0.004
C4	0.625	0.473	0.148	0.182	0.260	0.024
B9	0.839	0.496	0.208	0.263	0.330	0.043
B8	0.823	0.495	0.204	0.070	0.123	0.004
B4	0.635	0.475	0.151	0.154	0.232	0.018
B1	0.531	0.453	0.120	0.090	0.152	0.007
B5	0.638	0.476	0.152	0.161	0.240	0.019
B6	0.548	0.457	0.125	0.185	0.263	0.024
B7	0.597	0.468	0.140	0.190	0.268	0.025

Data with and without ouabain are given. f_{1W}, hydrogen bonded by one water molecule; f_{2W}, hydrogen bonded by two water molecules.

In all cases, the deuterium ^{2}H-ESEEM spectrum consists of a sharp component superimposed on a broad component. The sharp component arises from free D$_2$O molecules not H-bonded to the spin-label nitroxide -NO group, whereas the broad component is from D$_2$O molecules H-bonded to the nitroxide moiety (12). The total amplitude of the deuterium ESEEM signal, I_{tot}, is determined by the distance of the D$_2$O ^{2}H-nuclei from the spin label and by the number of D$_2$O molecules neighboring the spin label within 0.5 nm (12). This parameter, therefore, gives a direct measure of the extent of water (D$_2$O) penetration at the nitroxide-labeling site.

Fig. 6 reports ESEEM amplitudes I_{tot} and I_{broad} for the spin-labeled cinobufagins and bufalins incorporated in Na$^+$,K$^+$-ATPase membranes dispersed in D$_2$O in the absence and in the presence of excess ouabain. From Fig. 6, it is clearly evident that all spin-labeled cardiotonic steroids show a comparable high solvent (D$_2$O) intensity, indicating that the extracellular entrance to the ouabain binding site of the Na$^+$,K$^+$-ATPase is accessible to water. In particular, for bufalins **B1**, **B4**, **B5**, **B6**, and **B7**, I_{tot}(^{2}H) is ~220–230 ns and slightly higher for **B8** and **B9**, where I_{tot}(^{2}H) is ~245–260 ns. The three cinobufagin **C4**, **C8**, and **C9** have ^{2}H-ESEEM intensities comparable to those of the corresponding bufalins **B4**, **B8**, and **B9**, respectively. Displacement of each cardiotonic steroid from the binding cavity is accompanied by a large reduction in I_{tot}(^{2}H). The greatest difference, ΔI_{tot}(^{2}H) $\approx$ 215–225 ns, is found for bufalin **B8** and the corresponding cinobufagin **C8**, which have the shortest linker; a reduction of ΔI_{tot}(^{2}H) $\approx$ 185 ns is found for **B1**, whereas for all other bufalins, the difference lies between 115 and 145 ns.

Solvent properties: H-bond formation

Analysis of spin-label D$_2$O-ESEEM intensities gives information on H-bonding of water with the nitroxide -NO group (12). From the intensity of the broad component, which is due to nitroxides H-bonded to the solvent, it is possible to evaluate the product of equilibrium constant for hydrogen bonding, K, and effective concentration of free water, [W], $K \times$ [W], as well as the fraction of nitroxides that are singly (f_{1w}) and doubly (f_{2w}) bonded to D$_2$O as reported elsewhere (12).

Note that parallel studies quantitating resolved H-bonding states with high-field CW-EPR have confirmed the reliability of this method based on the ^{2}H-ESEEM intensities (26).

As can be seen from Table 1, values of the $K \times$ [W] product are in the range 0.5–0.8 for spin-labeled cardiotonic steroids in the cavity and are much reduced, in the range 0.2–0.4, for those bound to the membrane but displaced from the cavity. Correspondingly, f_{1w} is higher than f_{2w}, and both are higher for spin-labeled steroids in the binding site than at nonspecific loci in Na$^+$,K$^+$-ATPase membrane dispersions.
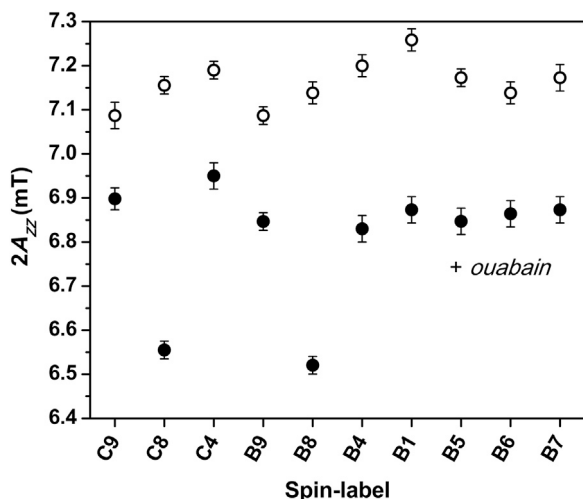
FIGURE 7 Outer hyperfine splitting, $2A_{zz}$, in the CW-EPR spectra of different spin-labeled cinobufagins and bufalins in Na^+,K^+-ATPase membranes in the absence (*open symbols*) and presence (*solid symbols*) of ouabain. $T = -196°C$. The data represent averages of three measurements with standard deviations.

The results in Table 1 highlight the difference in properties of the solvent at the entrance of the hydrophilic binding site in Na^+,K^+-ATPase (for samples in the absence of ouabain) and in the lipid membrane environment (for samples in excess ouabain).

^{14}N- hyperfine splitting

Pulsed D_2O-ESEEM results reported in Fig. 6 for direct water accessibility at the entrance to the binding site in Na^+,K^+-ATPase are complemented by probing environmental polarity at the spin-label locus based on measurements of the ^{14}N-hyperfine splitting constant, A_{zz}, at $-196°C$ (cf. 24,27). CW-EPR spectra in the absence and in the presence of ouabain are reported in Fig. S20, *A and B*, respectively. Corresponding values of A_{zz} for the various spin-labeled cardiotonic steroids in Na^+,K^+-ATPase are shown in Fig. 7.

For each cardiotonic steroid in the absence of ouabain, the nitroxide is located in a region of high polarity ($2A_{zz} \approx 7.1-7.2$ mT), consistent with the binding site being accessible to the aqueous phase (intense ^{2}H-signal). In the presence of excess ouabain, the reduction in water accessibility is mirrored by lower values of A_{zz}. Again, the biggest difference $2\Delta A_{zz} \approx 0.6$ mT is observed for **C8** and **B8**, which have the shortest linker, whereas for the other spin labels it lies in the range 0.2–0.4 mT.

Docking of the spin labels in the inhibitor site and analysis of the depth of water penetration

For each spin-labeled compound, the docking procedure resulted in a number of allowed poses (*N*) within the CTS

binding site of the Na^+,K^+-ATPase (Table S4). It appears that the orientation and position of the steroid cores of the bufalin spin labels (**B1**, **B4**, and **B7**) are very similar to bufalin in the crystal structure (PDB: 4RES) (see Fig. 8 *A*). As expected, positions of the nitroxide moiety vary with length of the flexible spacer arm. Although all are able to reach the loop connecting transmembrane segments $\alpha M7-\alpha M8$ (Fig. 8 *B*), the spacer arm of **B7** is long enough also to wrap around loop $\alpha M7-\alpha M8$ on either side (Fig. 8 *C*). Overall, the binding modes of **B4** and **B7** are highly similar to those reported for the cinobufagins **C4** and **C7** (8). The nitroxide of **B4** is located between the $\alpha M1-\alpha M2$ and $\alpha M7-\alpha M8$ loops, and **B7** can wrap around the $\alpha M7-\alpha M8$ loop either in the direction of the $\alpha M3-\alpha M4$ loop or in the direction of $\alpha M6$, as found for **C7**.

In contrast to **B1**, **B4**, and **B7**, the rather short and rigid linkers in compounds **B8**, **C8**, and **B9** prevent their pyrrolidine rings from getting close to the loops connecting transmembrane helices (Fig. S21). Note that compounds **B8**, **C8**, and **B9** score poorly in the docking algorithm because the empirical scoring function is based on the extent of ligand-protein contact. The linker and nitroxide of these compounds are exposed to solvent and do not interact with the protein, leading to artifactually low (i.e., positive) scores.

Predictions of the depth of water penetration into the site were done for the Na^+,K^+-ATPase-bufalin complex. Fig. 8 *D* depicts the cavity accessible for water molecules modeled as spheres with radius of 1.4 Å. This light gray area covers the CTS binding site, creating a continuous environment between the cation-binding sites and extracellular bulk phase. Fig. 8 *D* also illustrates that docking places spin labels of **B1**, **B7**, and **B8** within the water-filled area, in agreement with EPR data.

DISCUSSION

Conventional EPR lineshapes: label mobility in Na^+,K^+-ATPase binding site

The dynamic flexibility of the spin-label attachment probes the protein environment at the entrance to the inhibitor binding site. This depends, in turn, on the spin-label structure in several crucial aspects: the planar five-membered nitroxide ring (PROXYLs: **B8**, **B9**, and **C8**, **C9**) is rigid, whereas the six-membered ring (TEMPOs: **B1**, **B4**–**B7**, and **C4**) can undergo transitions between boat and chair conformations (see, e.g., (28).); the amide and carboxyl linkages are rigid (with partial double-bond character), whereas *trans-gauche* isomerism is found for methylene linkages and practically free rotation about ether bonds. The molecular axis system associated to the -NO nitroxide group is shown in Fig. S22. In this axis system, *x* lies along the N-O bond, *z* along the nitrogen p_π-orbital, and *y* is orthogonal to both.
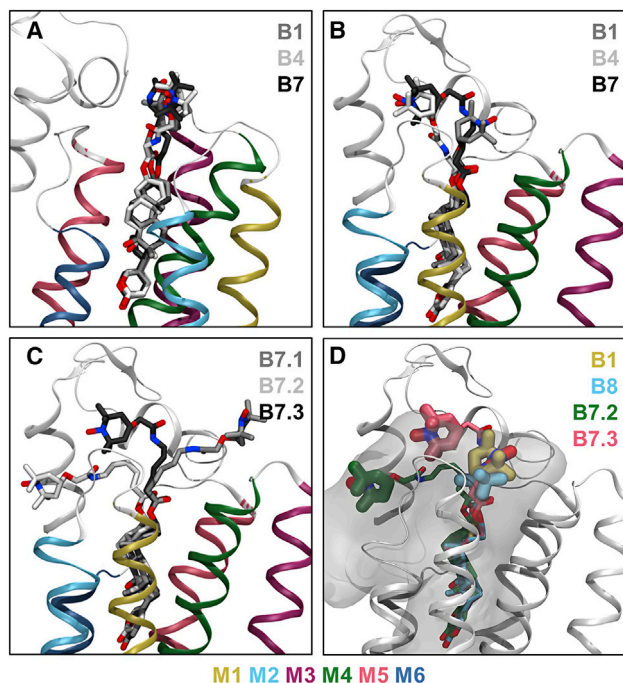
FIGURE 8 Binding modes of spin-labeled bufadienolides. (*A*) View from within the membrane with transmembrane segments αM1–4 on the right and αM5–6 as well as the αM7–αM8 loop on the left. (*B*) View rotated by ~90°, highlighting the ability of **B1**, **B4**, and **B7** to reach the αM7–αM8 loop despite their different linker lengths. (*C*) Different possible orientations of the nitroxide of **B7** (**B7.1**, **B7.2**, and **B7.3**) in the same view as (*B*). Protein backbone is shown as ribbons with transmembrane segments αM1–6 color coded as indicated. Longer loop between αM7 and αM8 is shown in light gray ribbons. (*D*) Nitroxide groups of **B1**, **B7**, and **B8** overlap with the water-filled area (*light gray surface*, same view as *C*). B7.1 is not shown because its nitroxide is fully exposed to the bulk solvent and thus not within the gray sphere representing the water-accessible area within the binding site.

Consider first the two PROXYL (i.e., five-membered-ring) nitroxides with spectra shown in Fig. 2. **B9** displays a practically rigid-limit lineshape; the link between nitroxide and steroid nucleus of bufalin contains a five-membered heterocycle and is essentially rigid. The characteristic EPR lineshape, therefore, indicates that bufalin (and also cinobufagin) is held rigidly within the ouabain inhibitor site (on the nanosecond timescale that characterizes conventional nitroxide EPR). **B8** with a shorter but potentially flexible linkage also has a spectrum characteristic of strong immobilization but less than the rigid limit of **B9**. This is confirmed by molecular docking. According to these calculations, spin labels of both **B8** and **B9** are not in contact with the protein, and their immobilization is due solely to rigid binding of the steroid core (Fig. S21). When compared with the shortest six-membered-ring bufalin, **B1** with only slightly longer link (*spectrum* shown in Fig. 3), we see extensive motional averaging attributable to rotation about the ether bond and conformational ring transitions, relative to the immobilized **B8**. This suggests that the vestibule im-

mediate to the binding site has sufficient volume to allow boat-chair transitions of the six-membered TEMPO ring with corresponding axial-equatorial interchange of the four methyl groups flanking the nitroxide (see later in this section for estimation of rates).

Concentrating now solely on the six-membered-ring nitroxides, whose spectra are shown in Fig. 3, we see a range in extent of motional averaging and different lineshapes depending on chemical structure of the nitroxide probe (see (28) and Fig. S22 for treatment of spin-label EPR lineshapes). That with the longest attachment, viz. **B7**, shows complete isotropic motional averaging. The length of attachment and number of bonds about which rotation can take place indicates that in this case, the nitroxide moiety is located at the entrance to the cavity leading to the bufalin binding site or beyond (see (9); Fig. 8). It is important to remember here that the spectra of cinobufagin analogs are essentially identical to those of the corresponding bufalin spin labels (Fig. 2). This shows that cinobufagin and the bufalin bind in the same way to the inhibitory site on the Na⁺,K⁺-ATPase. Small differences in the steroid core (affecting affinity) do not affect the position of the spin labels in the vestibuli.

Figs. 2 and 3 compare EPR lineshapes all at the same fixed temperature. For strongly immobilized spin labels (**B8** and **B9**) and those freely rotating (**B7**), lineshapes are likely to vary only quantitatively with temperature. In contrast, for nitroxides of intermediate mobility, temperature variation produces qualitative changes in lineshape that are indicative of the motional mode (see Fig. 4). For instance, the lineshapes of **B5** (and several other bufalin spin labels) are characteristic of preferential rotation about the nitroxide y axis (29–31). However, the lineshapes of **B4** indicate axially anisotropic rotation about the nitroxide z axis, and those of **B1** tend to show isotropic rotational diffusion with no preferential axis (see Fig. S22 for illustrative spectral simulations with uniaxial rotation). In all cases, preferential x axis rotation is excluded as the dominant motional mode because the low-field line is not the narrowest (i.e., of greatest height).

As mentioned, several of the different six-membered-ring nitroxides display y axis rotation, and one might ask why this is a preferred mode. One answer is that this is exactly the rotation that we expect for chair-boat conformational transitions of the six-membered piperidine ring. These produce concerted changes in orientation of the nitroxide z and x axes about the y axis (see Fig. S22) that are of sufficient amplitude to achieve complete angular averaging. As seen previously, these nitroxides are located in regions of the binding-site vestibule that have sufficient volume to accommodate the changes in methyl-group orientation that accompany transitions between chair and boat conformations.

Note that conformationally sensitive isotropic ¹³Cβ-hyperfine couplings of six-membered-ring nitroxides are consistent with fast exchange between ring conformers

(see (28), Section 3.7). The exchange rate needed for this is the angular frequency $\Delta\omega_{C\beta} \equiv 1/\tau > 155$ MHz (see (28), Eq. 3.33), whereas that for averaging the ^{14}N hyperfine anisotropy by y axis rotation is $\Delta\omega_{z\text{-}x} = (A_{zz} - A_{xx})/\hbar > 500$ MHz. The two lower limits are within a factor three and entirely consistent with boat-chair transitions producing characteristic y axis lineshapes such as that in Fig. S22. As implied already, comparison with the rigid five-membered-ring nitroxides demonstrates conformational averaging in the six-membered-ring nitroxides.

Conventional EPR lineshapes: inhibitor in lipid environments

Displacing spin-labeled inhibitor from the specific binding site by excess ouabain yields the spectra from inhibitors partitioning between aqueous phase and lipid environment of the membrane (Figs. 2, *lower panel*, and 3). Rapid diffusion within the lipid membrane plane (32,33) thus provides efficient two-dimensional channeling of inhibitor to the Na,K-ATPase before binding. Spectra of spin-labeled bufalins **B1**, **B4**, **B5**, **B6**, and **B7** and cinobufagins **C4** and **C8** reveal a motionally restricted component of inhibitors localized at the lipid-protein interface. This feature is common to lipid-protein interactions with the Na,K-ATPase and other large integral membrane proteins (21,23,34). It occurs whenever spin-label mobility in the fluid lipid environment is sufficient to allow spectral resolution of the restricted component (35–37), and extends not only to membrane lipids but also, for example, to spin-labeled aminated local anesthetics (38). Note that although inhibitors occupying the protein-lipid interface may not access the specific site directly, rapid binding ensues locally via the aqueous phase.

ESEEM intensities: water accessibility in inhibitor binding site

The ^{2}H-ESEEM spectra are qualitatively similar for the spin labels located at the inhibitor site and displaced into the membrane (by excess ouabain). They consist of a broad component from D_2O directly hydrogen bonded to the nitroxide group -NO and a narrow component from non-H-bonded D_2O molecules in the immediate vicinity (12). The ratio of broad/narrow components is similar in the presence and absence of ouabain, reflecting a similar H-bonding equilibrium in the binding site to that in the membrane. An important difference, however, is that the absolute values are much larger at the binding site than in the membrane. This is because the nitroxide situated in the membrane experiences a much lower local water concentration than that in the water-accessible vestibule at the inhibitor site. The latter is comparable to D_2O-ESEEM intensities found for spin labels attached to surface -SH groups on the Na$^+$,K$^+$-ATPase (39,40) and other proteins (41). In the membrane, intensities are comparable to those of lipids spin labeled at the $n = 6-8$

chain position, or $9-10$ for the short-linked **B8** and **C8** (9,42–44), and reflect the limited partitioning of water into the hydrophobic interior. In turn, this is reflected in relative values of the product $K[W]$ between H-bond association constant and free water concentration, which essentially becomes scaled by the water-membrane partition coefficient K_P, i.e., $K_{eff} = K \times K_P$. Correspondingly, the number of H-bonded spin labels is greater in the binding-site vestibule than in the membrane (Table 1).

Correspondences similar to those for water accessibility are found also for the polarity-dependent values of A_{zz} in the presence and absence of ouabain (39,42–44).

The most salient feature of the profiles of both water accessibility and local polarity is the remarkable constancy throughout the length of the vestibule to the binding site (Figs. 6 and 7). By contrast, the short-linked **B8** and **C8** spin labels, in the presence of ouabain, clearly sense the decreasing polarity and water accessibility of nitroxides situated deeper into the hydrophobic interior of the membrane (44,45). This implies that the entrance vestibule of the inhibitor and K$^+$-ion binding sites consists of a water-filled cavity that extends to the aqueous phase.

A further notable difference between the ESEEM spectra in the presence and absence of ouabain is that the relative intensity of the (matrix) proton ^{1}H-ESEEM signal at $\sim$15 MHz is smaller in the binding site than in the membrane (compare *upper* and *lower rows* in Fig. 5). In the latter case, this results from the high density of methylene groups contributed by the lipid chains, which produces a higher local concentration of H-atoms than that contributed by the protein side chains in the inhibitor-site entrance of the Na$^+$,K$^+$-ATPase.

CONCLUSIONS

In summary, small differences in the binding modes of bufalin and cinobufagin, as reflected in lower affinities for cinobufagin derivatives, do not affect the overall position of the spin labels in the Na$^+$,K$^+$-ATPase binding cavity when congruent derivatives of bufalin and cinobufagin are compared. The vestibule leading to the binding site of the CTS steroid core and accommodating the spin labels is filled with water molecules. These findings are the results of both molecular modeling and EPR experiments. In this context, a large increase in the anthroylouabain fluorescence upon its binding to the Na,K-ATPase must be a reflection of local hydrophobic interactions of the anthroyl-group and not of the overall hydrophobicity of the CTS binding site.

Throughout the entire length of the linkers (up to $\sim$2 nm), the minimal diameter of the vestibule allows rapid boat-chair conformational transitions of the six-membered nitroxide ring and accompanying rearrangements of the methyl groups. Because of the rigidity of their linkers, the five-membered probes **B8**–**B9** and **C8**–**C9** experience the restricted mobility of their steroid cores in the enzyme

binding site. All flexible linkers (**B4–B7**), despite their varying lengths, bring the nitroxide out as far as the αM7–αM8 loop. Isotropic motion of **B7** (as seen before for **C7** (9)) shows that the spin label reaches the bulk extracellular environment. Decreases in affinity of **B4–B7** for the Na,K-ATPase correlate with the length of the linker, suggesting that large hydrophilic substituents might pull up the steroid core and disturb electrostatic interactions of the lactone ring with the cation in the cation-binding site.

AUTHOR CONTRIBUTIONS

ACKNOWLEDGMENTS

REFERENCES

1. Morth, J. P., B. P. Pedersen, …, P. Nissen. 2007. Crystal structure of the sodium-potassium pump. *Nature.* 450:1043–1049.

2. Shinoda, T., H. Ogawa, …, C. Toyoshima. 2009. Crystal structure of the sodium-potassium pump at 2.4 A resolution. *Nature.* 459:446–450.

3. Glynn, I. M. 2002. A hundred years of sodium pumping. *Annu. Rev. Physiol.* 64:1–18.

4. Xu, Y., X. Liu, …, W. Schwarz. 2016. Inhibitory efficacy of bufadienolides on Na$^+$,K$^+$-pump activity versus cell proliferation. *Biochem. Biophys. Rep.* 6:158–164.

5. Fortes, P. A. 1977. Anthroylouabain: a specific fluorescent probe for the cardiac glycoside receptor of the Na-K ATPase. *Biochemistry.* 16:531–540.

6. Yatime, L., M. Laursen, …, N. U. Fedosova. 2011. Structural insights into the high affinity binding of cardiotonic steroids to the Na$^+$,K$^+$-ATPase. *J. Struct. Biol.* 174:296–306.

7. Laursen, M., L. Yatime, …, N. U. Fedosova. 2013. Crystal structure of the high-affinity Na$^+$K$^+$-ATPase-ouabain complex with Mg^{2+} bound in the cation binding site. *Proc. Natl. Acad. Sci. USA.* 110:10958–10963.

8. Laursen, M., J. L. Gregersen, …, N. U. Fedosova. 2015. Structures and characterization of digoxin- and bufalin-bound Na$^+$,K$^+$-ATPase compared with the ouabain-bound complex. *Proc. Natl. Acad. Sci. USA.* 112:1755–1760.

9. Guo, J. H., R. W. Jiang, …, N. U. Fedosova. 2018. Spin-labeled derivatives of cardiotonic steroids as tools for characterization of the extracellular entrance to the binding site on Na$^+$, K$^+$ -ATPase. *FEBS J.* 285:2292–2305.

10. Castillo, J. P., H. Rui, …, M. Holmgren. 2015. Mechanism of potassium ion uptake by the Na(+)/K(+)-ATPase. *Nat. Commun.* 6:7622.

11. Klodos, I., M. Esmann, and R. L. Post. 2002. Large-scale preparation of sodium-potassium ATPase from kidney outer medulla. *Kidney Int.* 62:2097–2100.

12. Erilov, D. A., R. Bartucci, …, L. Sportelli. 2005. Water concentration profiles in membranes measured by ESEEM of spin-labeled lipids. *J. Phys. Chem. B.* 109:12003–12013.

13. Bartucci, R., R. Guzzi, …, D. Marsh. 2009. Intramembrane water associated with TOAC spin-labeled alamethicin: electron spin-echo envelope modulation by D$_2$O. *Biophys. J.* 96:997–1007.

14. Sastry, G. M., M. Adzhigirey, …, W. Sherman. 2013. Protein and ligand preparation: parameters, protocols, and influence on virtual screening enrichments. *J. Comput. Aided Mol. Des.* 27:221–234.

15. Ladefoged, L. K., B. Schiøtt, and N. U. Fedosova. 2021. Beneficent and maleficent effects of cations on bufadienolide binding to Na$^+$,K$^+$-ATPase. *J. Chem. Inf. Model.* 61:976–986.

16. Shelley, J. C., A. Cholleti, …, M. Uchimaya. 2007. Epik: a software program for pK($_a$) prediction and protonation state generation for drug-like molecules. *J. Comput. Aided Mol. Des.* 21:681–691.

17. Kaminski, G. A., R. A. Friesner, …, W. L. Jorgensen. 2001. Evaluation and reparametrization of the OPLS-AA force field for proteins via comparison with accurate quantum chemical calculations on peptides. *J. Phys. Chem. B.* 105:6474–6487.

18. Friesner, R. A., R. B. Murphy, …, D. T. Mainz. 2006. Extra precision glide: docking and scoring incorporating a model of hydrophobic enclosure for protein-ligand complexes. *J. Med. Chem.* 49:6177–6196.

19. Paramo, T., A. East, …, P. J. Bond. 2014. Efficient characterization of protein cavities within molecular simulation trajectories: trj_cavity. *J. Chem. Theory Comput.* 10:2151–2164.

20. Marsh, D. 1981. Electron spin resonance: spin labels. *In* Membrane Spectroscopy. Molecular Biology, Biochemistry and Biophysics E. Grell, ed. . Springer Verlag, pp. 51–142.

21. Marsh, D., and L. I. Horváth. 1998. Structure, dynamics and composition of the lipid-protein interface. Perspectives from spin-labelling. *Biochim. Biophys. Acta.* 1376:267–296.

22. Marsh, D. 2018. Distinct populations in spin-label EPR spectra from nitroxides. *J. Phys. Chem. B.* 122:6129–6133.

23. Esmann, M., and D. Marsh. 2006. Lipid-protein interactions with the Na,K-ATPase. *Chem. Phys. Lipids.* 141:94–104.

24. Bartucci, R., D. A. Erilov, …, D. Marsh. 2006. Time-resolved electron spin resonance studies of spin-labelled lipids in membranes. *Chem. Phys. Lipids.* 141:142–157.

25. Dzuba, S. A., and D. Marsh. 2015. ESEEM of spin labels to study intermolecular interactions, molecular assembly and conformation. *In* Electron Paramagnetic Resonance B. C. Gilbert, V. Chechik, and D. M. Murphy, eds. . Royal Society of Chemistry, pp. 102–121.

26. Urban, L., and H. J. Steinhoff. 2013. Hydrogen bonding to the nitroxide of protein bound spin labels. *Mol. Phys.* 111:2873–2881.

27. Marsh, D. 1980. Molecular motion in phospholipid bilayers in the gel phase: long axis rotation. *Biochemistry.* 19:1632–1637.

28. Marsh, D. 2020. Spin-Label Electron Paramagnetic Resonance Spectroscopy. CRC Press, New York.

29. Polnaszek, C. F., D. Marsh, and I. C. P. Smith. 1981. Simulation of the ESR spectra of the cholestane spin probe under conditions of slow axial rotation: application to gel phase dipalmitoyl phosphatidylcholine. *J. Magn. Reson.* 43:54–64.

30. Schreier-Muccillo, S., D. Marsh, …, C. P. Smith. 1973. A spin probe study of the influence of cholesterol on motion and orientation of phospholipids in oriented multilayers and vesicles. *Chem. Phys. Lipids.* 10:11–27.

31. Marsh, D. 2010. Spin-label EPR for determining polarity and proticity in biomolecular assemblies: transmembrane profiles. *Appl. Magn. Reson.* 37:435–454.

32. Sachse, J.-H., M. D. King, and D. Marsh. 1987. ESR determination of lipid diffusion coefficients at low spin-label concentrations in biological membranes, using exchange broadening, exchange narrowing, and dipole-dipole interactions. *J. Magn. Reson.* 71:385–404.

33. Esmann, M., and D. Marsh. 1992. Local translational diffusion rates of membranous Na$^+$,K$(^+)$-ATPase measured by saturation transfer ESR spectroscopy. *Proc. Natl. Acad. Sci. USA.* 89:7606–7609.

34. Esmann, M., A. Watts, and D. Marsh. 1985. Spin-label studies of lipid-protein interactions in (Na$^+$,K$^+$)-ATPase membranes from rectal glands of *Squalus acanthias. Biochemistry.* 24:1386–1393.

35. Marsh, D. 2008. Electron spin resonance in membrane research: protein-lipid interactions. *Methods.* 46:83–96.

36. Esmann, M., and D. Marsh. 1985. Spin-label studies on the origin of the specificity of lipid-protein interactions in Na$^+$,K$^+$-ATPase membranes from *Squalus acanthias. Biochemistry.* 24:3572–3578.

37. Arora, A., M. Esmann, and D. Marsh. 1998. Selectivity of lipid-protein interactions with trypsinized Na, K-ATPase studied by spin-label EPR. *Biochim. Biophys. Acta.* 1371:163–167.

38. Horváth, L. I., H. R. Arias, …, D. Marsh. 1990. Association of spin-labeled local anesthetics at the hydrophobic surface of acetylcholine receptor in native membranes from *Torpedo marmorata. Biochemistry.* 29:8707–8713.

39. Guzzi, R., R. Bartucci, …, D. Marsh. 2009. Conformational heterogeneity and spin-labeled -SH groups: pulsed EPR of Na,K-ATPase. *Biochemistry.* 48:8343–8354.

40. Guzzi, R., M. Babavali, …, D. Marsh. 2011. Spin-echo EPR of Na,K-ATPase unfolding by urea. *Biochim. Biophys. Acta.* 1808:1618–1628.

41. De Simone, F., R. Guzzi, …, R. Bartucci. 2007. Electron spin-echo studies of spin-labelled lipid membranes and free fatty acids interacting with human serum albumin. *Biochim. Biophys. Acta.* 1768:1541–1549.

42. Aloi, E., and R. Bartucci. 2019. Solvent accessibility in interdigitated and micellar phases formed by DPPC/Lyso-PPC mixtures: D$_2$O-ESEEM of chain labeled lipids. *Chem. Phys. Lipids.* 221:39–45.

43. Oranges, M., R. Guzzi, …, R. Bartucci. 2018. Ether-linked lipids: spin-label EPR and spin echoes. *Chem. Phys. Lipids.* 212:130–137.

44. Bartucci, R., R. Guzzi, …, D. Marsh. 2014. Water penetration profile at the protein-lipid interface in Na,K-ATPase membranes. *Biophys. J.* 107:1375–1382.

45. Marsh, D. 2001. Polarity and permeation profiles in lipid membranes. *Proc. Natl. Acad. Sci. USA.* 98:7777–7782.